Research on Chemical Intermediates (2022) 48:3129–3142
https://doi.org/10.1007/s11164-022-04744-3

Selective hydrogenation of unsaturated aldehydes over Pd catalyst supported on N-doped porous carbon

Simin Sun[1] · Deng Pan[1] · Huijiang Huang[1] · Zheng Wang[1] · Yan Xu[1] · Yujun Zhao[1]

Received: 8 April 2022 / Accepted: 14 May 2022 / Published online: 9 June 2022

Abstract

Selective hydrogenation of unsaturated aldehydes is one of the most important reactions in organic chemical industry. Herein, a N-doped Pd catalyst supported on porous carbon (Pd/NC) was prepared and examined on selective hydrogenation of 2-ethyl-2-hexenal (EHEA) to 2-ethylhexanal (EHA). The N-doped Pd/NC catalyst shows a superior catalytic conversion (i.e., about 1.4 times higher than that on the counterpart Pd/C catalyst at 353 K) and a remarkable selectivity (98%) to hydrogenating C=C bond on EHEA to the saturated product (2-ethylhexanal). The catalyst characterization results suggest that N doping can promote the electron density on the surface of Pd, which enhances the adsorption and further activation of hydrogen molecules so that it significantly improves the hydrogenation rate of 2-ethyl-2-hexenal. It is also clarified that the by-product, 2-ethylhexanol is formed via the hydrogenation of C=C bond in 2-ethyl-2-hexenol rather than the C=O group in 2-ethylhexanal. These interesting findings provide a promising strategy for future catalyst design and a meaningful understanding of selective hydrogenation of unsaturated aldehydes on Pd catalyst.

Keywords Hydrogenation · Unsaturated aldehydes · N dopant · Pd · Porous carbon

Simin Sun and Deng Pan contribute equally as first author.

✉ Yan Xu
xuyan040506@tju.edu.cn

✉ Yujun Zhao
yujunzhao@tju.edu.cn

[1] Key Laboratory for Green Chemical Technology of Ministry of Education, School of Chemical Engineering and Technology, Tianjin University, Tianjin 300072, China

Introduction

The selective hydrogenation of unsaturated aldehydes is a critical step in the synthesis process of fine chemicals, pharmaceuticals, and functional materials since it has extensive applications [1–3]. In this reaction system, two different chemical pathways are involved and their major difference lies on the first step before fully hydrogenated to saturated alcohol: selective hydrogenation of the carbon–carbon double bonds (C=C) or the C=O bonds, as shown in Scheme 1 for selective hydrogenation of unsaturated aldehydes with EHEA as the model reactant [4, 5]. As a relatively low bond energy is required in the C=C hydrogenation in comparison with C=O hydrogenation, it is thermodynamically preferred [6]. The conjugated construction of the C=C and C=O bonds, in some ways, makes selective C=C hydrogenation more difficult, leading to the mixture of aldehyde, saturated, and unsaturated alcohol in the products.

Generally speaking, the hydrogenation selectivity of the unsaturated aldehyde is related to the *d*-bandwidth of the active metal because the interactions between the C=C and the active metal can be achieved easier on the active metal with a narrower *d*-bandwidth [1, 4, 7]. Among the noble metal catalysts used in the selective hydrogenation of C=C and C=O bonds, the Pd-based one has exhibited superior catalytic performance [8–11]. The narrow *d*-bandwidth of Pd results in a promising selectivity on C=C hydrogenation [12]. Besides, several approaches have been employed to further increase the selectivity of C=C hydrogenation, which include the use of bimetallic catalysts [10, 13], modified supports [14, 15], regulating the size of metal nanoparticles [12]. According to Zhang et al. [10] a selectivity as high as 99% for C=C hydrogenation can be achieved on the Pd–Au/CeO_2 catalyst. The alloy structure, which has a strong connection between Pd and Au, was found to facilitate the adsorption and activation of the C=C bond, hence increasing the hydrogenation of the C=C bond. Han et al. [13] developed a variety of Pd–Ni/SBA-15 bimetallic catalysts and applied them in the reaction of cinnamaldehyde selective hydrogenation. It achieves a conversion of 96.3% and a selectivity of 87.8% to hydrocinnamaldehyde. The improved Pd dispersion and synergistic effect between Ni and Pd nanoparticles are believed contributed to the

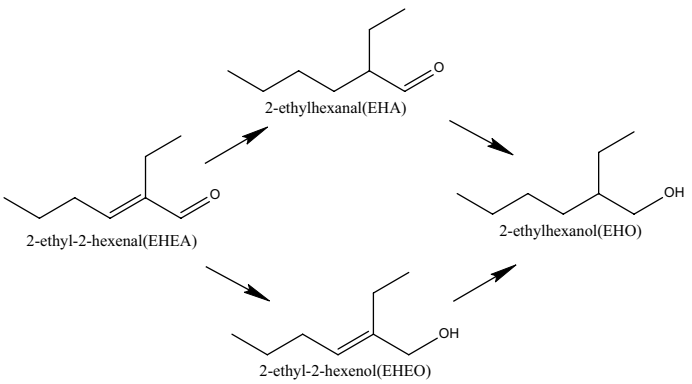

Scheme 1 Possible reaction routes of the hydrogenation of EHEA

excellent hydrogenation performance. According to Jiang et al. [12] smaller Pd nanoparticles provided a higher hydrogenation selectivity of C=C bonds. Their DFT calculations also confirmed that the C=C adsorption is favored on smaller Pd nanoparticles, while the C=O prefers to be adsorbed on a flat Pd surface.

Nitrogen-doped carbon materials have attracted numerous attentions and applied widely in different energy-related fields including supercapacitors, batteries, and catalyst supports [16–22]. Many researchers have clarified that the introduction of nitrogen element can not only create more structure defects to anchor metal nanoparticles, improve the metal dispersion, but also promote the electron density of the palladium species [14, 15]. Wei et al. [14] investigated hierarchically porous carbon with N-doping supporting Pd nanoparticles. A complete conversion of different kinds of unsaturated carbonyls was accomplished with extremely high selectivity (> 99%) under a mild condition (303 K, 1 MPa). The excellent performance of catalyst was ascribed to the introduction of N atoms and hierarchically porous structure. Li et al. [23] came up with a post-synthesis method to prepare N-functionalized ordered mesoporous carbon for loading Pd catalyst. The doped nitrogen atoms were found to be able to well disperse the Pd nanoparticles and stabilize their small size. The catalytic performance in the selective hydrogenation of phenol to cyclohexanone was enhanced due to the weak interactions between the N atoms and phenol molecules. With similar rationale, Wu et al. [24] demonstrated that Pd catalyst supported on a hierarchical porous N-doped carbon exhibited excellent stability toward the formation of 4-aminophenol through the reduction of 4-nitrophenol at ambient temperature. The coordination effect of doped nitrogen can help stabilize Pd nanoparticles on the carbon support. Nie et al. [15] treated graphene oxides by simple urea-hydrothermal method to obtain reduced graphene oxides (rGO) containing nitrogen. The Pd nanoparticle catalyst loaded on this support showed a better selectivity to C=C bond saturation in the hydrogenation of cinnamaldehyde. A high selectivity of 96.5% was achieved at 70 °C and 2 MPa of H_2 with the conversion of 99%. The interaction between N and Pd atoms can improve Pd dispersion by anchoring Pd nanoparticles of ~ 1.6 nm. However, up to now, few research related to the hydrogenation of EHEA is reported on the use of Pd catalyst and the nitrogen doping effect in aldehyde hydrogenation. To explore its potential in selective hydrogenation of EHEA, in this work, Pd-based catalyst was prepared by choosing N-doped porous carbon as the support. The as-prepared catalyst was characterized by XRD, TEM, H_2-TPD and other methods (detailed characterization are described in Supporting Information (SI)). The catalytic performance was studied in the selective hydrogenation of EHEA to EHA, and the synergistic effect of nitrogen atoms and Pd catalyst was discussed.

Experiment

Catalyst preparation

All chemicals were bought from commercial suppliers, and the details are shown in Supporting Information (SI). We adopted a hard template method to prepare porous

carbon support. Typically, 5.87 g formaldehyde was added in 1.63 g deionized water to form a solution in which 0.054 g Na_2CO_3 was added. This is followed by dissolving 4 g resorcinol and 0.075 g melamine in the prepared solution under ultrasonic condition. Then, about 20 mL silica sol was added dropwise into the mixture which was moderately stirred at 38 ℃ for 3 h. After that, we dehydrated the received sample for 72 h at 85 ℃ and calcined it under 800 ℃ for 2 h in a flow of Ar atmosphere to get the N-doped carbon material. The carbon material was then treated in a solution of NaOH under 80 ℃ for 5 h to ensure the complete removal of silica. After further drying at 110 ℃ overnight, porous carbon material was obtained and denoted as NC. As for comparison, porous carbon without nitrogen dopant was prepared in the same way without adding melamine.

We adopted a strong electrostatic adsorption method (SEA) to prepare Pd/NC catalyst [25, 26]. Typically, the as-prepared N-doped porous carbon was dispersed in the ammonium hydroxide solution and weighted amount of $Pd(NH_3)_4Cl_2{\cdot}H_2O$ was slowly added into the above-mentioned solution under magnetic stir. Afterward, the suspension was magnetically stirred at 25 ℃ for 8 h with the pH value kept at 10 ~ 11. Then, the suspension was filtered and dried at 105 ℃ for 11 h. The obtained catalyst was reduced under 250 ℃ for 2 h in H_2 flow. After cooled to ambient temperature, the above catalyst was treated with 1% O_2–Ar for 30 min. The as-prepared catalyst was denoted as Pd/NC. In the same way, we prepared porous carbon supported catalyst without nitrogen dopant, named by Pd/C. The mass loading of Pd was 0.45 wt% for all the catalysts.

Catalytic performance

The hydrogenation reactions were carried out in a 100-mL high-pressure autoclave (AB100-C276, ShanghaiLABE Instrument Co., Ltd) to evaluate the performance of two catalysts. Generally, 0.05 g passivated catalyst was added into the autoclave with 0.8 g EHEA as the substrate and 24.2 g *n*-hexane as the solvent. Prior to testing, we purged the sealed autoclave with hydrogen for five times so that the air inside can be completely removed. The experiment was carried out at 353 K, 2 MPa under stirring of 600 rpm for 4 h. The reaction mixture was analyzed using the gas chromatograph (BEIFEN 3420A) equipped with FID. The selectivity and conversion were calculated by following equations:

$$\text{Conversion} = \frac{(\text{moles of EHEA})_{\text{in}} - (\text{moles of EHEA})_{\text{out}}}{(\text{moles of EHEA})_{\text{in}}} \tag{1}$$

$$\text{Selectivity} = \frac{\text{moles of product } i}{\sum \text{moles of products}} \tag{2}$$

$$\text{TOF}_{\text{Pd}} = \frac{m_{\text{EHEA}} \cdot M_{\text{Pd}} \cdot \text{conv}}{M_{\text{EHEA}} \cdot t \cdot m_{\text{cat.}} \cdot \text{Wt}_{\text{Pd}} \cdot D_{\text{Pd}}} (\text{mol}_{\text{EHEA}} \cdot \text{mol}_{\text{Pd}}^{-1} \cdot \text{h}^{-1}) \tag{3}$$

m_{EHEA}: the mass of EHEA (g); conv: the conversion of EHEA (%); M_{EHEA}: the molecule weight of EHEA (g/mol); t: reaction time (h); m_{cat}: the mass of catalyst (g); Wt_{Pd}: the mass loading of Pd (%); D_{Pd}: the dispersion of Pd (%); M_{Pd}: the molecule weight of Pd (g/mol).

Results and discussion

Physicochemical properties of the catalysts

N_2 adsorption/desorption isotherms and the calculated pore size distribution of those catalysts are shown in Fig. 1. All four samples show type IV isotherms with H4 hysteretic loop, which demonstrates the existence of both micropores and mesopores. Both porous carbon supports and catalysts show a peak in the range of 0.5–0.6 nm (Fig. 1b) about the pore size distribution curves, indicating all the pore size distributions are relatively concentrated. The pore size distribution in Fig. 1c confirms the existence of mesopores at about 10–30 nm in the carbon supports, which were formed by removing the silica particles during the NaOH solution treatment. In addition, the specific surface area of N-doped porous carbon is 767 m^2/g, which is smaller than that of the porous carbon (1075 m^2/g) without N doping (Table 1). It indicates that the N doping affects the construction of the carbon structure. Moreover, the Pd/C presents a lower specific surface area than its support, implying that part of the pores is blocked by Pd nanoparticles during the metal loading process. It is noteworthy that Pd/NC and NC exhibit almost identical specific surface area, suggesting that the loading of Pd has no negative effect on the N-doped carbon support.

The inclusion of N and Si is essential to the catalyst. According to the HRTEM-EDS results, the nitrogen content of Pd/NC is quantified to be 1.01% (Table 1). Meanwhile, thermogravimetric (TG) is conducted on both carbon supports. Figure 2 shows that the weight loss of both supports start at 400 °C and stop at 530 °C. The residue of the samples is SiO_2, whose weight is 3.29% and 2.56% of the initial mass of the supports. It indicates that the SiO_2, as the hard template agent for the construction of the mesopores in carbon materials, has been almost completely removed.

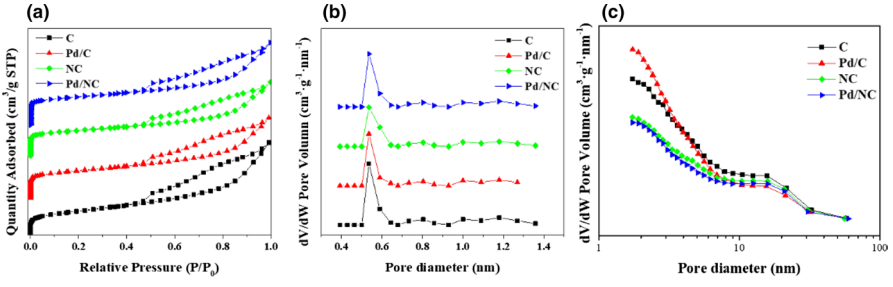

Fig. 1 N_2 adsorption–desorption isotherms (**a**), pore size distribution (**b**) and pore size distribution of BJH (**c**)

Table 1 Physicochemical properties of the supports and catalysts

Sample	SSA[a] (m^2/g)	Volume$_{micro}$[a] (m^3/g)	Volume[a] (m^3/g)	Pd[b] wt./%	N[c] wt./%	Dispersion[d]/%
C	1075	0.25	1.15	–	–	–
Pd/C	834	0.19	0.89	0.45	–	69.7
NC	767	0.17	0.80	–	0.99	–
Pd/NC	755	0.18	0.90	0.46	1.01	68.9

[a]Determined by N_2 isotherm adsorption–desorption, [b]determined by ICP-OES, [c]determined by HRTEM-EDS, [d]determined by HRTEM

In order to explore the Pd dispersion on the catalyst support, HRTEM was conducted and the particle size distribution of Pd nanoparticles was measured. There is no obvious difference in the morphologies of Pd/C and Pd/NC catalysts, both of which are amorphous (Fig. S1). As shown in Fig. 3, both reduced catalysts show ultrasmall Pd nanoparticle sizes, which can be attributed to the advantage of the SEA method for metal loading. The average nanoparticle sizes of both Pd/C and Pd/NC catalysts are about 1.6 nm. The Pd dispersion on the two catalysts determined by HRTEM is 69.7% and 68.9%, respectively. Obviously, the introduction of N atoms has no significant effect on the Pd dispersion, which can be ascribed to the high specific surface area of carbon and low mass content of Pd. Additionally, the images of HRTEM as well as energy dispersive spectroscopy (EDS) of reduced Pd/NC catalyst further reveals the spatial distribution of Pd and N. As shown in Fig. 4, Pd as well as N is dispersed evenly on the carbon support, which further indicates that N has been successfully doped into the skeleton of porous carbon and Pd nanoparticles were highly dispersed.

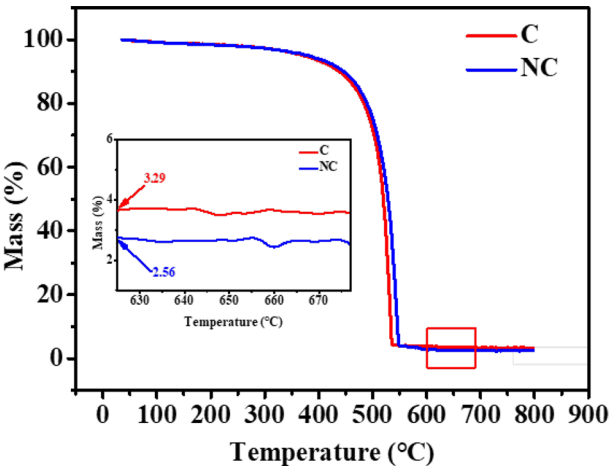

Fig. 2 TG analysis curves of two types of carbon support

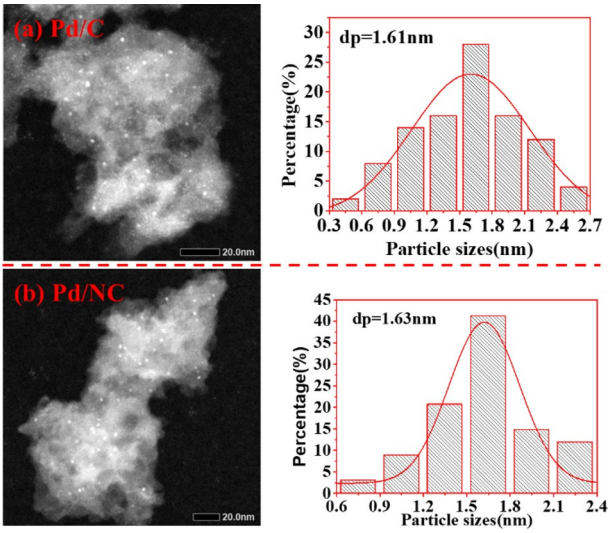

Fig. 3 HRTEM images of reduced catalysts Pd/C (**a**) and Pd/NC (**b**)

Figure 5 displays the XRD patterns of C, NC, Pd/C and Pd/NC. The broad characteristic diffraction peak at about 23° and 44° could be assigned to (100) and (002) planes of typical amorphous carbon, respectively [27, 28]. The characteristic diffraction peak of Pd didn't appear on the reduced catalysts because of the high dispersion

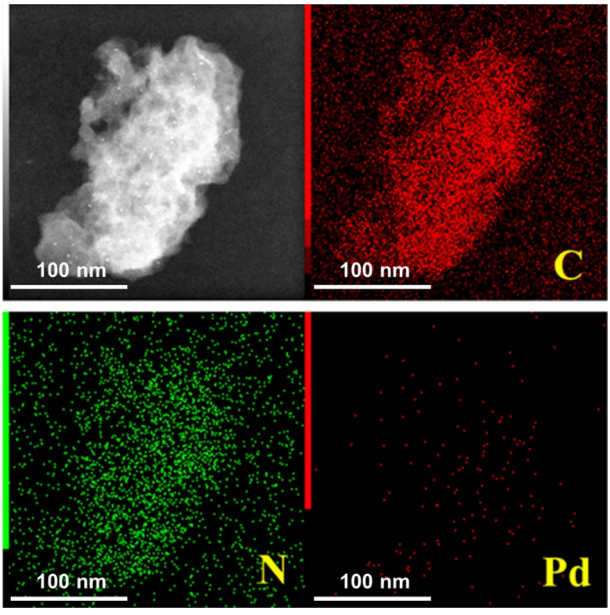

Fig. 4 HRTEM-EDS mapping images of the reduced Pd/NC catalyst

while low mass loading of Pd—the nanoparticle size of which is smaller than the detectable limit (generally ~ 3 nm). These results agree well with the HRTEM results.

Effect of N doping on chemical state

The FTIR spectra of the two types of porous carbon support are shown in Fig. 6. The broad peak between 900 and 1300 cm^{-1} is assigned to the stretching vibration of C–O group from various ethers, alcohols, and phenols [29, 30]. The peak at about 1573 cm^{-1} belongs to the stretching vibration of aromatic C=C bond [31]. There is no obvious characteristic peak for N–O or N–H because of the limited amount of N dopant in those carbon supports [32].

H_2-TPD was conducted to examine the ability of those catalysts in hydrogen adsorption. As shown in Fig. 7, each sample shows three desorption peaks. The desorption peak at about 85 °C is attributed to the weak adsorption of hydrogen on both catalysts. With the N doping into porous carbon, the hydrogen desorption peak at 389 ℃ and 456 ℃ on Pd/C catalyst shifts to 396 ℃ and 464 ℃, respectively, implying a stronger adsorption of hydrogen on the N-doped Pd catalyst [33]. It can be deduced that N dopant enhanced the adsorption of hydrogen on the catalyst [34], which could improve the catalytic performance of Pd in C=C hydrogenation.

XPS was applied for evaluating the surface chemical states of Pd on different catalysts. The binding energy of the reduced catalysts has been calibrated by the C 1 s spectra. As shown in Fig. 8, the peak at 341.7 eV is assigned to the metallic Pd $3d_{3/2}$ on the Pd/C catalyst. When doping nitrogen in the porous carbon support, the peak of Pd $3d_{3/2}$ shifts to a lower BE (~ 0.6 eV), which suggests the electronic migration between Pd nanoparticles and porous carbon. The oxidized Pd species also has a negative shift (~ 0.5 eV). According to the reports, the nitrogen-doped carbon can serve as an electron donor. It would cause electron transfer to Pd so that the Pd nanoparticles would get higher electron density and consequently the binding energy

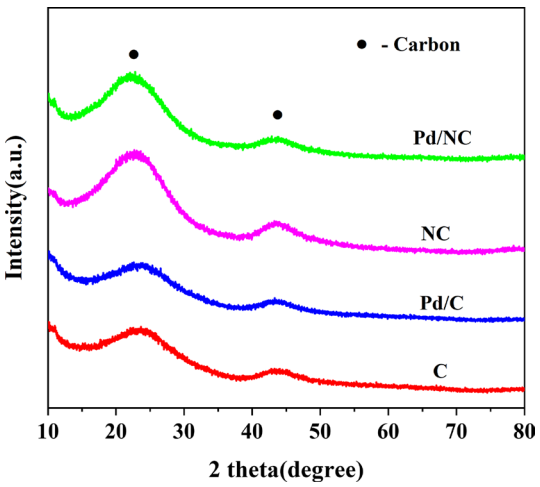

Fig. 5 XRD patterns of porous carbon and reduced catalysts

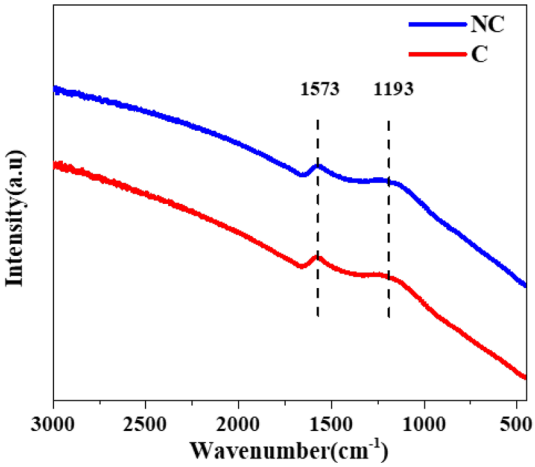

Fig. 6 FTIR spectra of two types of support

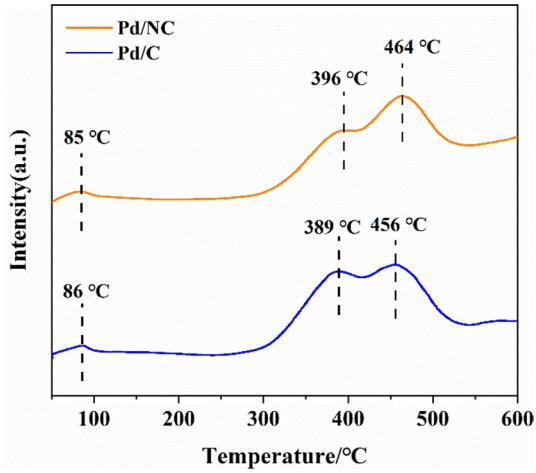

Fig. 7 H_2-TPD profiles of Pd/NC catalyst and Pd/C catalyst

of Pd 3d decreases [35–39]. It can be also confirmed by the XPS N 1 s spectrum of Pd/NC catalyst (Fig. S2). After the deconvolution of the main peak, one peak at the binding energy of 398.9 eV is found, which is assigned to the lone-pair N atom having interaction with Pd (Pd–N) [40, 41]. It also proves that nitrogen is successfully doped into the porous carbon support. The increase of the electron density on Pd surface can contribute to the adsorption and dissociation of hydrogen molecules, which can further improve the catalytic performance in hydrogenation.

Catalytic performance

The selective hydrogenation of EHEA to EHA was used to evaluate the catalytic performance. As shown in Fig. 9a, the conversion of EHEA on Pd/C and Pd/NC is

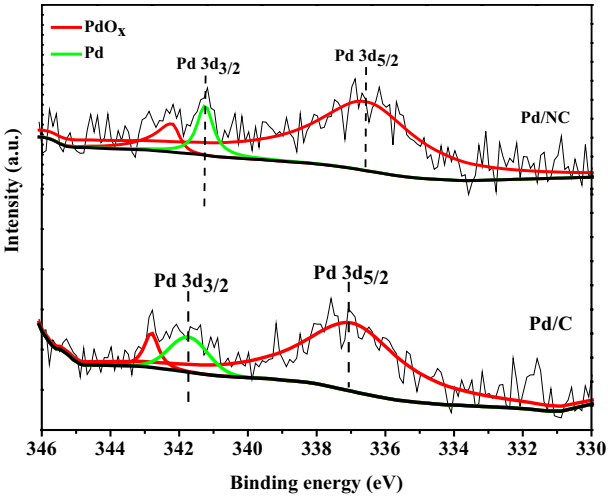

Fig. 8 Pd 3d XPS spectra of both reduced catalysts

45.6% and 65.5%, respectively. N-doped Pd catalyst shows a superior catalytic performance, which is around 1.4 times as high as that of Pd/C. But the two catalysts give almost similar selectivity to EHA (~98%) (Table S1). Considering that the dispersion of Pd on the Pd/NC catalyst is similar to that on the Pd/C, a higher catalytic performance of Pd/NC catalysts must be ascribed to other reasons. On basis of the XPS results, the dopant nitrogen can serve as an electron donor, which transfers electrons to Pd nanoparticles, improving the electron density of surface Pd. On the one hand, proved by the H_2-TPD results, the enrichment of electrons on the surface of Pd contributes to the adsorption and activation of hydrogen. On the other hand, the electron-rich surface inevitably increases the repulsion between C=C bond and Pd nanoparticles, suppressing the adsorption of C=C group of unsaturated aldehydes.

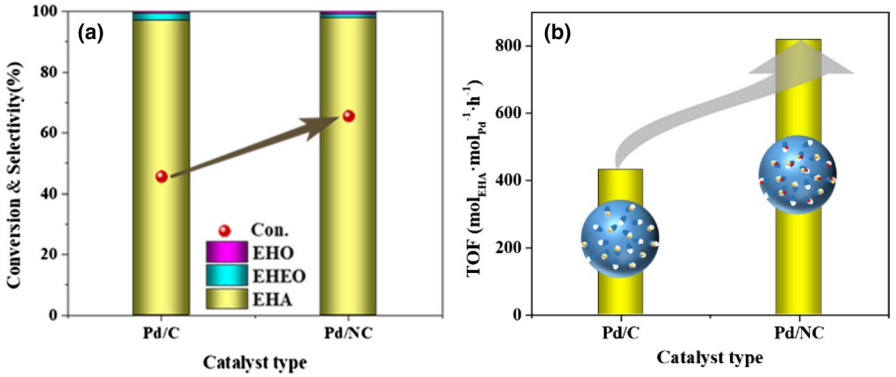

Fig. 9 Catalytic performances on both catalysts: conversion and selectivity (**a**); TOF values (**b**). Reaction conditions: catalyst = 0.05 g; P = 2 MPa; WLHSV = 4 h^{-1}; t = 4 h; T = 353 K

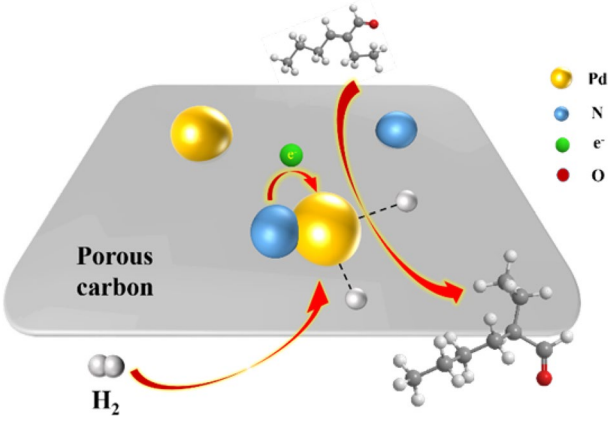

Scheme 2 The proposed process during the hydrogenation reaction

Therefore, the adsorption and activation of hydrogen could be the rate-determining step in selective hydrogenation of EHEA to EHA on the Pd/NC catalyst.

The TOF values of both catalysts were further calculated and are shown in Fig. 9b. Obviously, the TOF value of Pd site gets significantly improved when the porous carbon support is doped by N. It further indicates that the electrons transfer from dopant nitrogen to Pd nanoparticles enhances the adsorption and activation of hydrogen, which should be the rate-determining step for hydrogenation process. This promotion effect of nitrogen was also reported by Cao et al. that supporting N-doped carbon nanotubes (CNT) with Pd nanoparticles exhibited excellent activity in the selective hydrogenation of acetylene because nitrogen doping could tailor the electronic density of Pd and thus improving the kinetics of the partial hydrogenation of acetylene [42]. According to above results, a mechanism is proposed for the catalytic behavior of Pd/NC in EHEA hydrogenation. As shown in Scheme 2, electrons transfer from N dopant to adjacent Pd nanoparticles, increasing the electron density of the surface Pd nanoparticles, which greatly enhances the adsorption and activation of hydrogen. Then, the adsorbed H atoms on Pd surface, after dissociation, can react with the adsorbed EHEA molecules to facilitate the selective conversion to EHA.

Reaction pathways

Because of the presence of both C=O and C=C bonds in EHEA molecule, it is essential to obtain an insightful understanding of the real reaction pathways of this reaction system. As shown in Fig. 10 and Table S2, the selectivity of EHA remains constant with extended reaction time even at an EHEA conversion of 98%. This implies that further hydrogenation of EHA to EHO on the Pd catalyst is relatively difficult at the given reaction condition. Therefore, trace EHO is mainly formed via the hydrogenation of the C=C bond in EHEO rather than the C=O bond in EHA. In another word, the formation of EHO follows a different and parallel pathway from

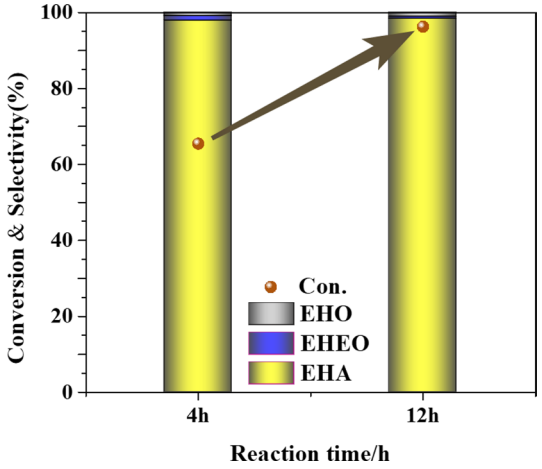

Fig. 10 Reaction results of EHEA hydrogenation at different reaction times

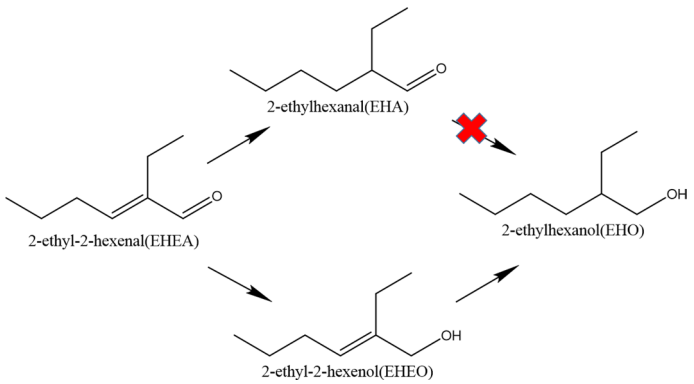

Scheme 3 Reaction pathways of EHEA hydrogenation

that of the formation of EHA (Scheme 3). Jiang et al. reported that the rate of C=C hydrogenation in cinnamyl alcohol is quite fast, about 30 times higher than that of the hydrogenation of C=O in hydrocinnamaldehyde [12]. It indicates that the hydrogenation of C=O group will be difficult once C=C bond in EHEA is firstly hydrogenated. As a result, the selectivity of EHA is almost a constant at about 98% even when the conversion of EHEA is very high.

Conclusion

In our work, N-doped porous carbon support was prepared and the Pd nanoparticles were loaded on such supports by SEA method. The catalyst with N dopant shows a better catalytic performance, which is about 1.4 times as high as the Pd/C catalyst. The N dopant increases the electron density of the surface Pd, promoting the adsorption and activation of hydrogen molecules, which is believed the rate-determining

step of this hydrogenation reaction. Meanwhile, it is also confirmed that the by-product EHO was produced by the hydrogenation of the C=C bond in EHEO rather than the C=O bond in EHA. Because the hydrogenation of the former bond (C=O bond) is much more difficult than the latter (C=C bond in EHEA), a significantly high yield of EHA (98%) was achieved on the Pd/NC catalyst. These findings provide meaningful understanding of the selective hydrogenation of unsaturated aldehydes and useful guidance on catalyst design in this reaction system.

Supplementary Information The online version contains supplementary material available at https://doi.org/10.1007/s11164-022-04744-3.

Acknowledgements We are grateful for the financial support from the National Natural Science Foundation of China (21878227).

Funding National Natural Science Foundation of China, 21878227, Yujun Zhao.

References

1. J.M. Grosselin, C. Mercier, G. Allmang, F. Grass, Organometallics **10**, 7 (1991)
2. P. Mäki-Arvela, J. Hájek, T. Salmi, D.Y. Murzin. Appl. Catal. A Gen. **292**, (2005)
3. X. Lan, T. Wang, X. Li, N. Huang, J. Wang, Catal. Sci. Technol. **6**, 21 (2016)
4. F. Delbecq, P. Sautet, J. Catal. **152**, 2 (1995)
5. X. Lan, T. Wang, ACS Catal. **10**, 4 (2020)
6. X. Wang, X. Liang, P. Geng, Q. Li, ACS Catal. **10**, 4 (2020)
7. F. Delbecq, P. Sautet, J. Catal. **211**, 2 (2002)
8. J. Ma, L. Xu, L. Xu, H. Wang, S. Xu, H. Li, S. Xie, H. Li, ACS Catal. **3**, 5 (2013)
9. D. Wang, Y. Zhu, C. Tian, L. Wang, W. Zhou, Y. Dong, H. Yan, H. Fu, ChemCatChem **8**, 9 (2016)
10. Y. Zhang, X. Yang, Y. Zhou, G. Li, Z. Li, C. Liu, M. Bao, W. Shen, Nanoscale **8**, 44 (2016)
11. S. Chen, L. Meng, B. Chen, W. Chen, X. Duan, X. Huang, B. Zhang, H. Fu, Y. Wan, ACS Catal. **7**, 3 (2017)
12. F. Jiang, J. Cai, B. Liu, Y. Xu, X. Liu, RSC Adv. **6**, 79 (2016)
13. S. Han, Y. Liu, J. Li, R. Li, F. Yuan, Y. Zhu, Catalysts **8**, 5 (2018)
14. Z. Wei, Y. Gong, T. Xiong, P. Zhang, H. Li, Y. Wang, Catal. Sci. Technol. **5**, 1 (2015)
15. R. Nie, M. Miao, W. Du, J. Shi, Y. Liu, Z. Hou. Appl. Catal. B Environ. **180**, (2016)
16. R.K. Abasabadi, A.A. Khodadadi, Y. Mortazavi, Res. Chem. Intermed. **47**, 4 (2021)
17. L. Wu, Y. Long, J. Ma, G. Lu, Res. Chem. Intermed. **45**, 7 (2019)
18. N. Guo, M. Li, Y. Wang, X. Sun, F. Wang, R. Yang, RSC Adv. **6**, 103 (2016)
19. I. Ziccarelli, H. Neumann, C. Kreyenschulte, B. Gabriele, M. Beller, Chem. Commun. **52**, 86 (2016)
20. Y. Cao, B. Zhao, X. Bao, Y. Wang, ACS Catal. **8**, 8 (2018)
21. X. Xu, M. Tang, M. Li, H. Li, Y. Wang, ACS Catal. **4**, 9 (2014)
22. S. Ott, A. Orfanidi, H. Schmies, B. Anke, H.N. Nong, J. Hübner, U. Gernert, M. Gliech, M. Lerch, P. Strasser, Nat. Mater. **19**, 1 (2020)
23. Z. Li, J. Liu, C. Xia, F. Li, ACS Catal. **3**, 11 (2013)
24. X. Wu, H. Zhou, New J. Chem. **41**, 18 (2017)
25. F. Wang, K. Han, L. Xu, H. Yu, W. Shi, Ind. Eng. Chem. Res. **60**, 8 (2021)
26. L. Zhang, G. Wen, H. Liu, N. Wang, D.S. Su, ChemCatChem **6**, 9 (2014)
27. L.-L. Wang, L.-P. Zhu, N.-C. Bing and L.-J. Wang. J. Phys. Chem. Solids **107**, (2017)
28. W.A. Wang, H. Huang, B. Wang, C. Qian, P. Li, J. Zhou, Z. Liang, C. Yang, S. Guo, Sci. Bull. **64**, 21 (2019)
29. Y. Yang, D. Zeng, S. Shao, S. Hao, G. Zhu, B. Liu. J. Colloid Interf. Sci. **538**, (2019)
30. J. Zawadzki, M. Wiśniewski, K. Skowrońska, Appl. Catal. B Environ. **35**, 4 (2002)
31. M. Trchová, E.N. Konyushenko, J. Stejskal, J. Kovářová, G. Ćirić-Marjanović, Polym. Degrad. Stabil. **94**, 6 (2009)

32. Y. Zhu, G. Yu, J. Yang, M. Yuan, D. Xu and Z. Dong. J. Colloid Interf. Sci. **533**, (2019)
33. Z. Chunhui, Z. Yifeng, L. Huazhang, J. Rare Earths **28**, 4 (2010)
34. L. Ma, P. Chen, G. Zhang, L. Wang, F. Tang, X. Zhao, J. Wang, J. Huang, Y.N. Liu, ChemCatChem **13**, 14 (2021)
35. Y. Chen, J. Wang, H. Liu, M.N. Banis, R. Li, X. Sun, T.-K. Sham, S. Ye, S. Knights, J. Phys. Chem. C **115**, 9 (2011)
36. M. Jeon, K.-S. Lee, S.H. Choi, J. Han, S.W. Nam, S.C. Jang, H.S. Park, C.W. Yoon, Int. J. Hydrog. Energy **41**, 34 (2016)
37. Y.-H. Qin, Z.-Y. Xiong, J. Ma, L. Yang, Z. Wu, W. Feng, T.-L. Wang, W.-G. Wang, C.-W. Wang, Int. J. Hydrog. Energy **42**, 2 (2017)
38. G. Wu, C. Dai, D. Wang, D. Li, N. Li, J. Mater. Chem. A **20**, 15 (2010)
39. Z. He, B. Dong, W. Wang, G. Yang, Y. Cao, H. Wang, Y. Yang, Q. Wang, F. Peng, H. Yu, ACS Catal. **9**, 4 (2019)
40. G. Wang, S. Yuan, Z. Wu, W. Liu, H. Zhan, Y. Liang, X. Chen, B. Ma, S. Bi, Appl. Organomet. Chem. **33**, 11 (2019)
41. J. Yang, X. Qi, F. Shen, M. Qiu, R.L. Smith Jr. Sci. Total Environ. **719**, (2020)
42. Y. Cao, W. Fu, Z. Ren, Z. Sui, J. Zhou, J. Luo, X. Duan, X. Zhou, AICHE J. **66**, 4 (2020)